Amplification of Xenon NMR and MRI by Remote Detection

Adam J. Moulé, Megan M. Spence[1], Song-I Han, Juliette A. Seeley, Kimberly L. Pierce, Sunil Saxena[2], and Alexander Pines*

Materials Science Division, Lawrence Berkeley National laboratory and Department of Chemistry, University of California, Berkeley, CA 94720, USA.

* To whom correspondence should be addressed. pines@cchem.berkeley.edu

[1] Laboratorium für Physikalische Chemie, E.T.H. Zürich, 8093 Zürich, Switzerland.

[2] Department of Chemistry, University of Pittsburgh, Pittsburgh, PA 15260, USA.

A novel technique is proposed in which a nuclear magnetic resonance (NMR) spectrum or magnetic resonance image (MRI) is encoded and stored as spin polarization and is then moved to a different physical location to be detected. *Remote detection* allows the separate optimization of the encoding and detection steps, permitting the independent choice of experimental conditions, and excitation and detection methodologies. In the first experimental demonstration of this technique, we show that NMR signal can be amplified by taking diluted ^{129}Xe from a porous sample placed inside a large encoding coil, and concentrating it into a smaller detection coil. In general, the study of NMR active molecules at low concentration that have low physical filling factor is facilitated by remote detection. In the second experiment, MRI information encoded in a very low field magnet (4-7 mT) is transferred to a high field magnet (4.2 T) in order to be detected under optimized conditions. Furthermore, remote detection allows the utilization of ultra-sensitive optical or superconducting detection techniques, which broadens the horizon of NMR experimentation.

In a conventional NMR experiment, a series of radio frequency (rf) and gradient pulses are applied to the information carrying sample nuclei immersed in a strong magnetic field in order to encode information about the local atomic environment, physical interactions between the nuclei, and the macroscopic position and motion of the nuclei of interest. The encoded information is then detected through the observation of the resulting frequencies and amplitudes. A single rf coil is commonly used for both the encoding and detection (*1*) of the NMR signal, so that only one aspect can be optimized to the detriment of the other. So, conventional NMR employs a compromise that is a trade-off between encoding and detection efficiency, resulting in conditions that are not necessarily optimal for either mode. We present a new technique, NMR remote detection, that separates the encoding and detection steps both spatially and temporally. The NMR information is carried by means of longitudinal magnetization from one location to the other. NMR remote detection capitalizes on the extraordinary

strength of NMR, the myriad of encoding possibilities, and suggests new experimental paths to circumvent the inherent weak point of NMR, the low sensitivity.

The unique feature of remote detection is that information encoded about the sample at one location is detected at a different location. The remote detection pulse sequence is based on the principle of indirect detection (*2, 3*), and generally consists of three segments, the encoding period, the travel or mixing period, and the detection period (fig. 1A). In the simplest case (fig. 1B), the encoding step is a $\pi/2$ excitation pulse followed by an evolution period t_1 and a $\pi/2$ storage pulse. The transverse magnetization evolves during t_1 under a given Hamiltonian, and its projection along x or y (depending on the phase of the storage pulse) is stored as longitudinal information by the second pulse. The stored longitudinal magnetization is transferred to the detection coil by physically moving the stored magnetization between locations. The amplitude of the stored magnetization is determined using a $\pi/2$ pulse in the detection coil. By incrementing the t_1 evolution time, the NMR time domain signal is modulated along the indirect dimension (fig. 3C). The spectrum or image that is encoded in the first coil is reconstructed in the second coil using point-by-point detection. The principle of remote detection is generally applicable to NMR experiments where coherence carries the NMR information. One drawback is that this indirect acquisition inherently adds one dimension to the remote experiment.

Several different scenarios for the application of the remote detection principle exist, which can be tailored to favor the experimental conditions. The most basic approach is the optimization of the filling factor of the detection coil, where the signal to noise ratio (SNR) can be enhanced without changing the encoding conditions. Particularly large samples such as human body cavities, and also small porous samples and bio-molecular solutions, often contain the information carrying nuclei in a very dilute concentration. The result is a poor filling factor for the NMR spins inside the encoding coil. These nuclei can be extracted from the medium, and physically concentrated into a smaller detection coil with an optimal filling factor and higher sensitivity (*4*). The detection of a signal from a large encoding volume with a smaller coil is performed either by multiple samplings over a longer time range to cover all of the encoded volume, or by physically condensing the encoded gas into the liquid- or solid-state.

The use of different magnetic fields for encoding and detection is another possibility for remote detection, and opens new perspectives for NMR. NMR image information is encoded at very low fields, which is favorable for imaging of heterogeneous objects due to lower susceptibility gradients (*5, 6*). The detection can then be performed in a high field magnet to achieve a better SNR. This approach makes the use of less homogeneous ultra-high field, permanent, and hybrid magnets (*7*), both viable and advantageous because only the encoding field, but not necessarily the detection field, needs to be very homogeneous.

Finally, remote detection is also naturally suited for another innovative step, namely to replace inductive coil detection by an alternative ultra-sensitive detection technique such as Superconducting QUantum Interference Device (SQUID) or optical detection. SQUIDs offer highly sensitive detection

for low frequency applications (*8*). If the carrier spins are ^{129}Xe gas, spin-exchange optical detection provides an extremely sensitive means to monitor the xenon polarization through contact with Rb metal vapor (*9*).

The carrier of remote information can be any NMR sensitive nuclei, provided that the longitudinal polarization survives the travel from the encoding location to the detection location. Various biological fluids or gases could be used as carriers of remote information, but the ideal carrier medium is hyper-polarized ^{129}Xe gas. A magnetic field independent xenon polarization on the order of several percent is produced via spin-exchange optical pumping of Rb vapor (*10*). The combination of high SNR, extremely long T_1 relaxation time, broad chemical shift range, and chemical inertness make ^{129}Xe atoms information carriers and model sensors of local environment (*11, 12*).

The favorable features of ^{129}Xe give access to void space MRI of the lung volume (*13*), chemical and structural properties of porous media (*14, 15*), and protein binding events in solution state (*16*). Also, MRI of dissolved phase xenon in a mammal‘s lung tissue has been obtained by Ruppert et. Al. (*17*). Here, a large bath of pre-polarized gaseous ^{129}Xe in the lung volume is utilized in order to amplify the signal of the dissolved xenon phase in the tissue, capitalizing on the rapid exchange between the two different environments. This method shares some basic concepts with remote detection, but not the aspects of controlled signal transfer or the explicit choice and optimization of the encoding and detection locations. Other examples in the literature, using an explicit two location approach for NMR, are the use of a flow apparatus for dynamic nuclear polarization experiments (*18*) or an elaborate pneumatic shuttling device for zero-field NMR (*19*).

The NMR signal transfer step necessitates the controlled flow of the encoded xenon nuclei during the course of each single NMR scan. A remarkable feature of remote detection is that nevertheless, irregularity and spreading of the flow pattern are, to a certain extent, not directly detrimental to the experiment. This is because the NMR time domain signal, not the NMR image or the NMR spectrum itself, is traveling. For each remote scan, the encoded signal can be collected in the detection coil by repeated acquisition which provide one remote data point in the time domain. Fourier transformation is performed on the complete remote data set, which provides the remotely detected NMR information.

After an appropriate flow rate is set, the travel time (t_t) between the encoding and detection locations, and the characteristic transport distribution of the signal must be determined. This has been measured by inverting the ^{129}Xe magnetization in the encoding coil, and then measuring the signal amplitude as it arrives in the detection coil after a certain incremented flow time. Examples of such travel time curves are presented in fig. 2. The timescale of t_t depends on the travel distance between two locations and the flow rate; fig. 2A corresponds to a travel distance of about 4 cm between two coils within one probe, and fig. 2B is measured for a travel distance of about 5 m between two different magnets (and coils) across the room from each other. Only positive amplitudes are observed because the inverted magnetization mixes with un-encoded magnetization due to diffusion and

turbulence while traveling. The minimum amplitude in each travel time curve corresponds to t_t, the time at which the greatest percentage of encoded signal has reached and occupied the detection cell. The broad dip around the minimum gives us information about the spread of encoded spins during the travel time.

The first experimental realization of high field remote detection spectroscopy was performed using a probe with two electronically isolated rf coils in the homogeneous region of the magnet with minimal travel distance between the coils. The larger diameter encoding coil was packed with Aerogel crystal fragments (fig. 3A). Aerogel (*20*) is a low density silicate that allows xenon gas to freely pass through its pore structure and leads to an approximately 30 ppm downfield chemical shift from the free gas peak due to adsorbed ^{129}Xe.

We successfully obtained the first remote chemical shift spectrum. The 1D remote spectrum in fig. 3D is a slice taken from the indirect dimension of the 2D NMR spectrum (fig. 3C). Because only pure xenon gas is transported (not the Aerogel sample itself) to the detection coil, the direct dimension shows a single xenon gas peak at 0 ppm, whereas the modulation of this direct peak (fig. 3C inset) measures the chemical shift of xenon gas inside the Aerogel fragments. The direct dimension represents the spectrum in the detection cell, and the indirect dimension the encoding cell. The three peaks in the remote spectrum (fig. 3D) correspond to the free ^{129}Xe gas peak, the bound gas peak and a reference peak which appears at zero on the figure scale. This reference peak arises due to un-encoded ^{129}Xe gas arriving at the detection coil, which leads to an offset in addition to the remote signal that cannot simply be corrected for because minute variations in the total ^{129}Xe polarization between each remote scan and T_1 noise lead to a fluctuation in the baseline offset. The remote spectrum shows a higher SNR ~33:1 (fig. 3D) than the directly detected spectrum from the encoding coil with a SNR of ~7:1 (fig. 3B), reflecting their filling factor difference of 4.6. This experiment demonstrates the signal amplification potential of remote detection, where information is read out in a more efficient way by transporting long living polarization to an optimized detector.

The second experimental demonstration of remote detection extends the basic idea in two senses. The acquisition of remote 2D images demonstrates that the relocation of a more complex information structure than a one dimensional spectrum is possible. Also, it shows that improvements, derived from the NMR conditions that exist at both low and high fields by encoding and detecting the signal at different magnetic fields, can be made. The first remote imaging experiments were performed using a low field magnet (4-7 mT) for the encoding site and a high field magnet (4.2 T) for the detection site (fig. 4A). The two sites were connected by Teflon tubing, and the travel distance for the remote signal was about 5 m. Typical travel times were 7-10 s for flow rates of 4-7 ml/s (fig. 2B). The sample cell at the encoding site is a glass container with a donut shaped restriction in its center. Fig. 4B,C shows 2D remote projections reconstructing images along the short and long axis of the sample taken from 3D remote experiments. The cross-sectional image is circular, showing the expected density distribution (fig. 4B), and the image depicting the long axis of the cell shows accurate length proportions with the

restriction at the correct location (fig. 4C). Also note that in fig. 4C the chambers on both sides of the restriction have the same SNR.

It is remarkable that NMR images, clearly representing the sample cell, can be reconstructed at all, after traveling a long distance under conditions where the spatial order of spin positions is lost. Remote imaging is possible because the encoded *k*-space data travels pixel by pixel after being stored as longitudinal magnetization, not its Fourier transformed data, which is the direct image information. Reconstruction of a full representation of position dependent spin densities requires that *all* the spins encoded in each remote scan, corresponding to one pixel in *k*-space, are relocated to the detection coil regardless of their macroscopic order. This "collection" is realized by multiple acquisitions. In remote imaging, blurring occurs mainly during the encoding period when the gas atoms diffuse and swap positions, as is also true for conventional gas phase imaging.

Whereas appropriate hardware is needed for conventional NMR at these low encoding fields (4-7 mT) in order to detect at audio frequencies, these low field remote images were detected utilizing the sensitivity and convenience of a standard high field spectrometer. Other advantages are that no electronic shielding is required for signal encoding and noise sources (e.g. produced from gradient amplifiers) can be neglected because the detection apparatus is far away. Inhomogeneous broadening due to susceptibility gradients are reduced three orders of magnitude at these low fields of a few millitesla compared to typical high field conditions of a few tesla.

The first experimental realization of remote NMR and MRI were demonstrated. Even the simplest remote spectroscopy experiment shows that, within the confines of T_1 relaxation time, the independently optimized experimental conditions for both the encoding and the detection site clearly lead to remote amplification of NMR signal. The remote imaging experiment shows that the relocation of more complex information structure than a one dimensional spectrum is indeed possible. The first remote image advantageously utilized vastly different fields to improve the resolution of encoding, through reduced susceptibility gradients, without the loss of high field detection capabilities. More generally, remote detection demonstrates that the separation of the previously interdependent encoding and detection steps provides a new pathway for further exploration of the limits of NMR.

Figure captions

Figure 1

(A) Remote detection begins with a pre-polarization step (*21*), followed subsequently by the three essential parts of the pulse sequence. They are the encoding of spectral or image information at on location, the transfer to a different location, and detection in the new location. (B) The pair of $\pi/2$ pulses are separated by t_1. The second $\pi/2$ pulse stores the evolved magnetization into the $\pm z$-direction. The stored magnetization is transferred to another location during t_t, and finally detected with a third

$\pi/2$ pulse. The encoding time, t_1 is incremented by the indirect dimension dwell time to map out NMR information in a point by point fashion.

Figure 2

The travel time curve plots the ^{129}Xe signal amplitude in the detection coil as a function of the *flow time*. After the magnetization is inverted in the encoding coil, the xenon signal travels from the encoding coil to the detection coil, and the resulting signal amplitude in the detection coil after a given flow time is read out. In (A), both coils are placed inside a high field magnet (7 T). It takes 28-60 ms for the encoded ^{129}Xe to travel a distance of about 4 cm from one coil to the other. In (B), the encoding coil is placed inside a low field magnet (4-7 mT), and the detection coil inside a high field magnet (4.2 T). Here, the encoded ^{129}Xe travels 7-10 s, corresponding to a distance of about 5 m from one magnet to the other.

Figure 3

(A) The first remote spectra were obtained using a home-built probe containing two coils that are separated by 2.5 cm, center to center, and by a copper sheet, which serves as an rf shield. A ¼" pyrex tube with a 180^o bend passes through both coils. The tubing in the lower coil (½" I.D) holds aerogel crystal fragments. The upper tubing section is empty and is centered within a ¼" I.D. coil. The two coils are controlled by separate *x*- and *y*-channels of a Varian Infinity Plus spectrometer tuned to 83.25 MHz. (B) Directly detected spectrum of ^{129}Xe in the encoding coil obtained with one $\pi/2$ pulse and one signal acquisition.

(C1) 2D time domain FID data of the 2D remote experiment. The direct dimension was obtained measuring 512 points with a dwell time of 50 μs, and in the indirect dimension, 256 points with a dwell time of 50 μs. One signal acquisition is used. The indirect dimension contains point-by-point detected FIDs, which are encoded in the encoding coil, and after signal transfer, remotely detected in the detection coil. Notice that the unencoded ^{129}Xe adds an apparent baseline offset to the indirectly detected FID.

(C2) 2D NMR spectrum of the 2D remote experiment. The direct dimension was obtained measuring 512 points with a dwell time of 50 μs, and in the indirect dimension, 256 points with a dwell time of 50 μs. One signal acquisition is used. The direct dimension contains one peak, representing the chemical shift information of the pure xenon gas inside the detection coil. The indirect dimension contains three peaks, representing the chemical shift information inside the encoding coil, which is remotely detected in the detection coil. The three peaks correspond to the pure xenon gas, the xenon gas absorbed to the inside surface of the Aerogel sample, and a reference peak due to baseline offset fluctuations.

(D) The remote spectrum represents one slice taken at the maximum gas peak of the direct dimension along the indirect dimension of the 2D data in fig. 3C2. The spectrum reconstructs the spectral information in the encoding coil although it is measured in the detection coil. Comparison of (B) and (D) shows that the remote experiment shows an SNR improvement of a factor of ~5x more than the directly detected spectrum due to the improved filling factor in the detection coil. (*22*)

Figure 4

(A) ^{129}Xe is polarized to 1-2% in a home built circular flow polarizer. Here, a gas mixture ratio of 1:2:3 for [Xe]:[N2]:[He] with a total pressure of 7 atm was used. Polarizer, encoding and detection sites were connected in a closed loop, maintaining a constant pressure of 7 atm (*23*). Xenon gas with a polarization of 1-2% was produced in a continuous flow mode (*24*). The low field magnet (4-7 mT, 129Xe frequency of 47.3-83.5 kHz) for the encoding site is a home built solenoid electromagnet (*25*) with a bore size of 29.8 cm. The high field detection takes place inside a 4.2 T (129Xe frequency of 49.8 MHz) super wide bore magnet equipped with a Chemagnetics spectrometer. The sample cell in the encoding site is a cylindrical glass (7 mm I.D.) tube with restrictions (donut shaped Teflon spacers) in the middle and at both ends. (*26*) (B) and (C) show two 2D remote detection images encoded at low field and detected at high field, together with sample schemes. The schematic diagrams show the dimensions of the glass sample tube and location of the restrictions, and also indicate the directions of the projection used for each image. For both images, the t_t was set to 7 s, corresponding to a flow rate of 6 ml/s and a traveling distance of about 5 m. Eighteen repeated detection pulses, separated by 0.15 s, are sequentially acquired to detect the entire encoded signal volume. The images are encoded using the technique of filtered back projection, which involves physically rotating the probe on a polar raster relative to the gradient coils (*27*). (B) shows a *yz* projection reconstruction image of the void space of the sample tube encoded at 4 mT. Eight projections separated by 22.5^o (128 points are acquired for each projection) are used for the reconstruction of the 2D image. Each projection is measured using a gradient strength of 1.23 mT/m, where the gradinet was oriented along a proscribed angle, yielding a nominal resolution of 1.2 mm in the 1D projection. (C) is a *xz* image encoded at 7 mT. The image was reconstructed from sixteen 1D projectiion (64 points for each projection). The same gradient strength as in (B) is used here. For data processing of both 2D images, the k-space data were zero-filled to 256 points before Fourier transformation.

References

1. D. I. Hoult, R. E. Richards, *Journal of Magnetic Resonance* **24**, 71-85 (1976).

2. J. Jeener, paper presented at the Proc. Ampere International Summer School II, Basko Polje, Yugoslavia 1971.
3. R. R. Ernst, G. Bodenhausen, A. Wokaun, *Principles of Nuclear Magnetic Resonance in One and Two Dimensions*, International Series of Monographs on Chemistry (Clarendon Press, Oxford, 1987), vol. 14.
4. D. L. Olson, T. L. Peck, A. G. Webb, R. L. Magin, J. V. Sweedler, *Science* **270**, 1967-1970 (Dec 22, 1995).
5. K. M. Ludeke, Roschmann, P. Tischler, R., *Magnetic Resonance Imaging* **3**, 329 (1985).
6. C. H. Tseng *et al.*, *Physical Review Letters* **81**, 3785-3788 (Oct 26, 1998).
7. M. D. Bird, Z. H. Gan, *Ieee Transactions on Applied Superconductivity* **12**, 447-451 (Mar, 2002).
8. Y. S. Greenberg, *Reviews of Modern Physics* **70**, 175-222 (Jan, 1998).
9. B. C. Grover, *Physical Review Letters* **40**, 391-392 (1978).
10. T. G. Walker, J. H. Thywissen, W. Happer, *Physical Review A* **56**, 2090-2094 (Sep, 1997).
11. C. I. Ratcliffe, *Annual Reports on NMR Spectroscopy* **36** (1998).
12. K. W. Miller *et al.*, *Proceedings of the National Academy of Sciences of the United States of America-Biological Sciences* **78**, 4946-4949 (1981).
13. M. S. Albert *et al.*, *Nature* **370**, 199-201 (Jul 21, 1994).
14. T. Ito, J. Fraissard, *Journal of Chemical Physics* **76**, 5225-5229 (1982).
15. J. L. Bonardet, J. Fraissard, A. Gedeon, M. A. Springuel-Huet, *Catalysis Reviews-Science and Engineering* **41**, 115-225 (1999).
16. M. M. Spence *et al.*, *Proceedings of the National Academy of Sciences of the United States of America* **98**, 10654-10657 (Sep 11, 2001).
17. K. Ruppert, J. R. Brookeman, K. D. Hagspiel, J. P. Mugler, *Magnetic Resonance in Medicine* **44**, 349-357 (Sep, 2000).
18. H. C. Dorn, R. Gitti, K. H. Tsai, T. E. Glass, *Chemical Physics Letters* **155**, 227-232 (Feb 24, 1989).
19. A. M. Thayer, A. Pines, *Accounts of Chemical Research* **20**, 47-53 (Feb, 1987).
20. S. Q. Zeng, A. Hunt, R. Greif, *Journal of Non-Crystalline Solids* **186**, 264-270 (Jun, 1995).
21. A. Macovski, S. Conolly, *Magnetic Resonance in Medicine* **30**, 221-230 (Aug, 1993).
22. . pp. The 129Xe, polarized to 1-5%, is produced using a commercial polarizer from Amersham Health. After the polarized gas is produced, it flows through the two coils sequentially and is later lost into the laboratory atmosphere. Gas flow rate is controlled using pressure differential through a silver coated needle valve and an on-board flow meter.
23. M. Haake, A. Pines, J. A. Reimer, R. Seydoux, *Journal of the American Chemical Society* **119**, 11711-11712 (Dec 3, 1997).
24. . pp. An ASCO three way gas flow valve is used to direct the flowing gas either through the magnets or to return to the inlet of the polarizer. The return line has an adjustable needle valve restriction so that a constant flow rate (and therefore a constant ^{129}Xe polarization) can be maintained in the pumping cell even during stop flow operation, which is necessary to allow sufficient encoding time.
25. D. Raftery, H. W. Long, D. Shykind, P. J. Grandinetti, A. Pines, *Physical Review A* **50**, 567-574 (Jul, 1994).
26. . pp. The pulses are gated and generated from a Hewlett Packard 3314A frequency generator and amplified to 8 Vp-p by an Amplifier Research 75 Watt unity gain amplifier for an experimental $\pi/2$ time of 48-70 μs. Three dimensional gradient coils are fixed on the outside of the magnet bore.

27. P. C. Lauterbur, *Nature* **242**, 190-191 (1973).

We thank C. A. Meriles for valuable discussions and A. H. Trabesinger and J. Urban for kindly reviewing the manuscript. This work was supported by the Director, Office of Science, Office of Basic Energy Sciences, Materials Sciences of the U.S. Department of Energy under Contract No. DE-AC03-76SF00098. S. Han gratefully acknowledges the Alexander von Humboldt Foundation for support through a postdoctoral fellowship.

Fig. 1

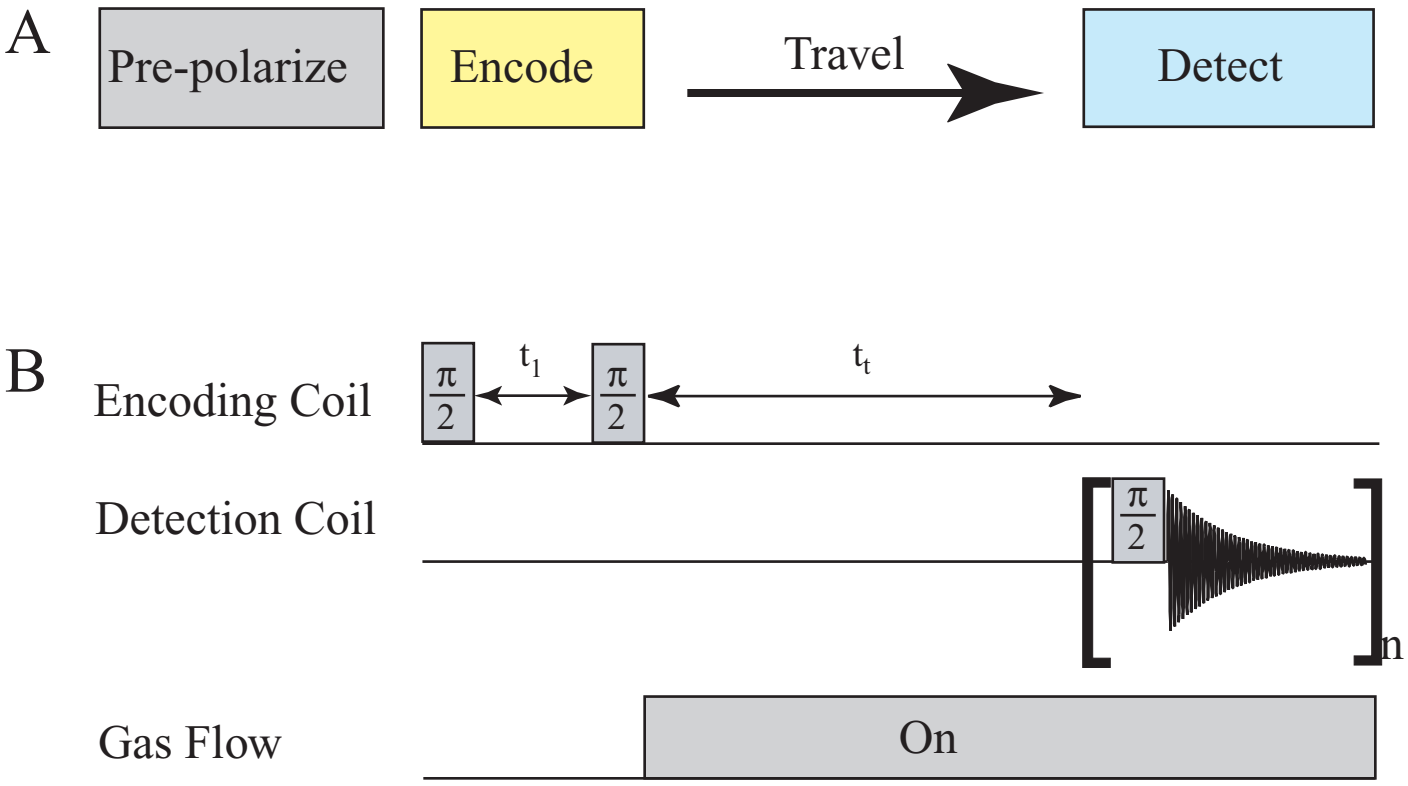
A
Pre-polarize
Encode
Travel
Detect
B
Encoding Coil
π/2
t1
π/2
tt
Detection Coil
π/2
n
Gas Flow
On

Fig. 2

A

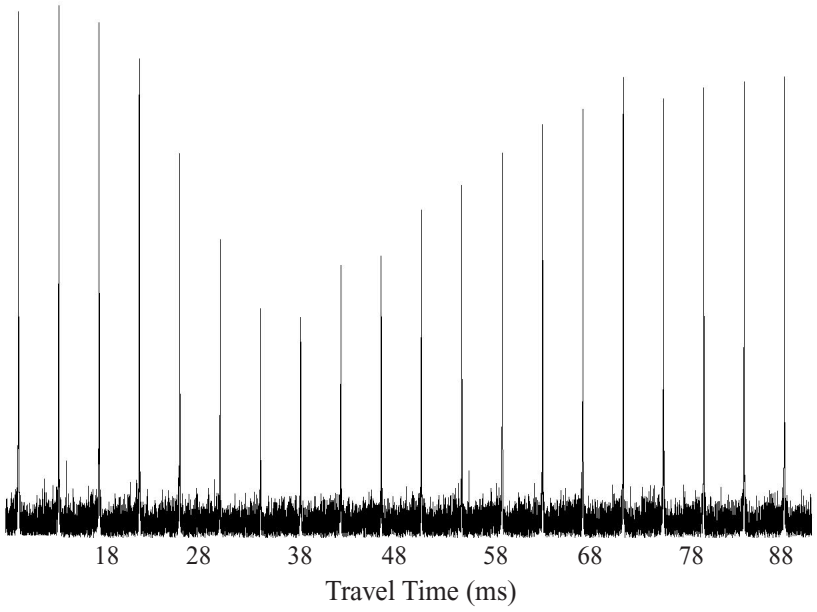
18
28
38
48
58
68
78
88
Travel Time (ms)

B

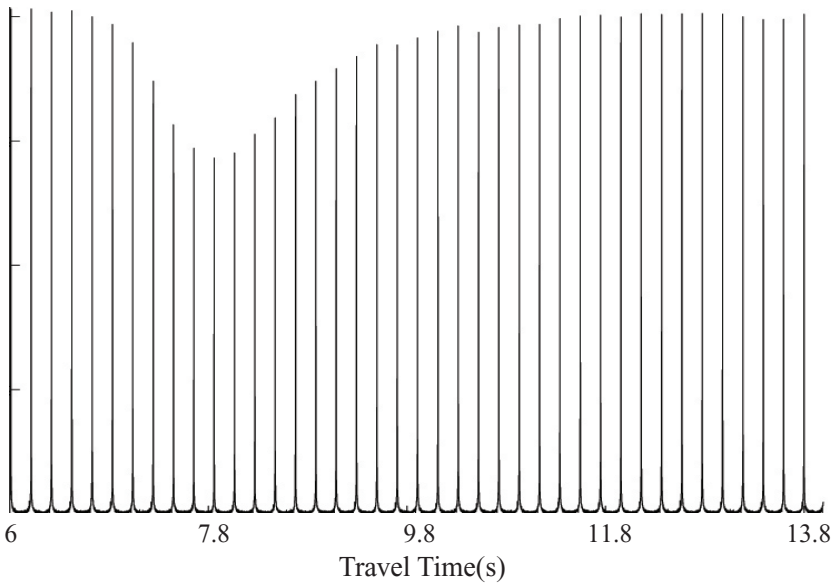
6
7.8
9.8
11.8
13.8
Travel Time(s)

Fig. 3

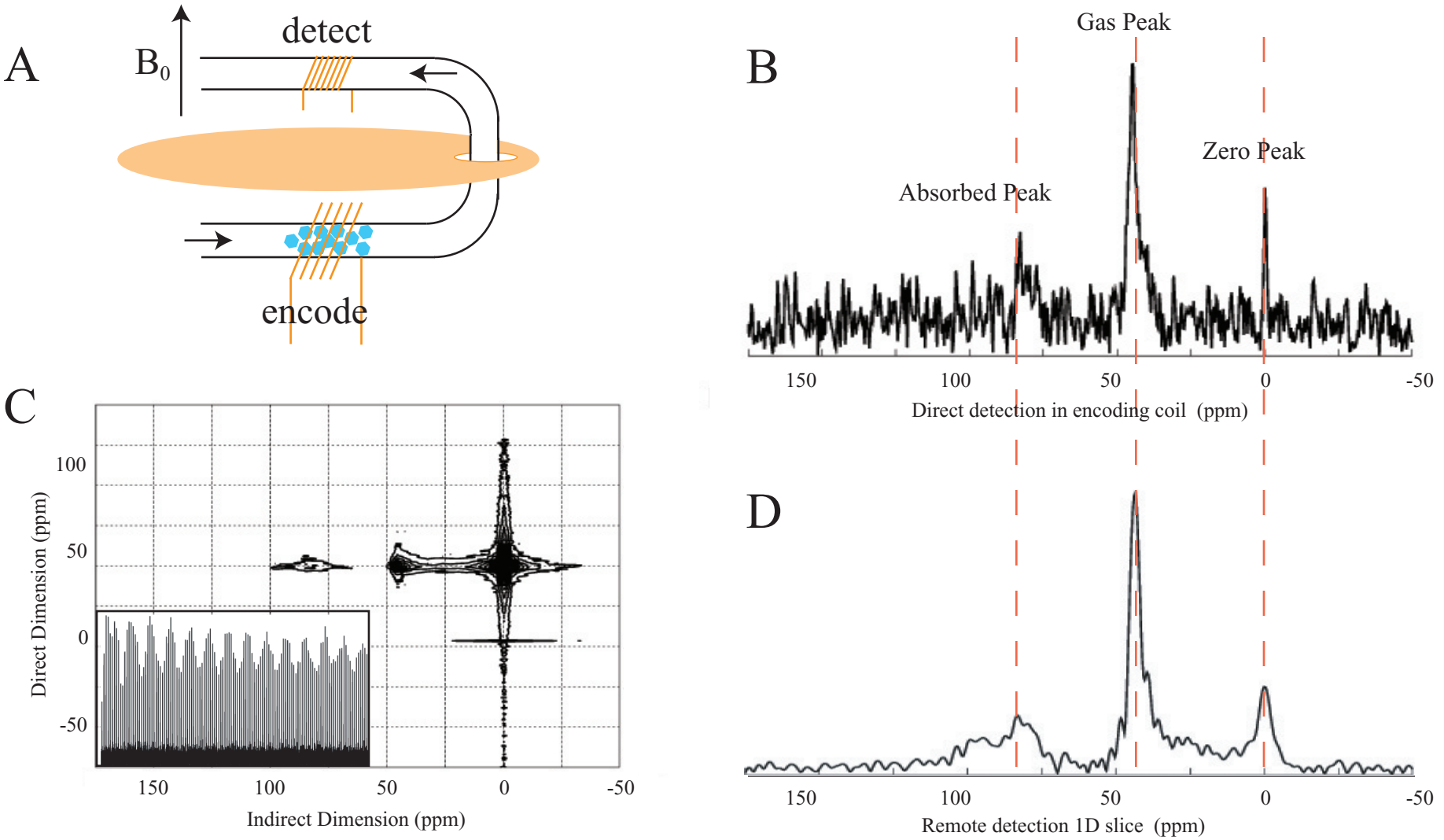
A
B0
detect
encode
B
Gas Peak
Zero Peak
Absorbed Peak
150
100
50
0
-50
Direct detection in encoding coil (ppm)
C
100
50
0
-50
Direct Dimension (ppm)
150
100
50
0
-50
Indirect Dimension (ppm)
D
150
100
50
0
-50
Remote detection 1D slice (ppm)

Fig. 4

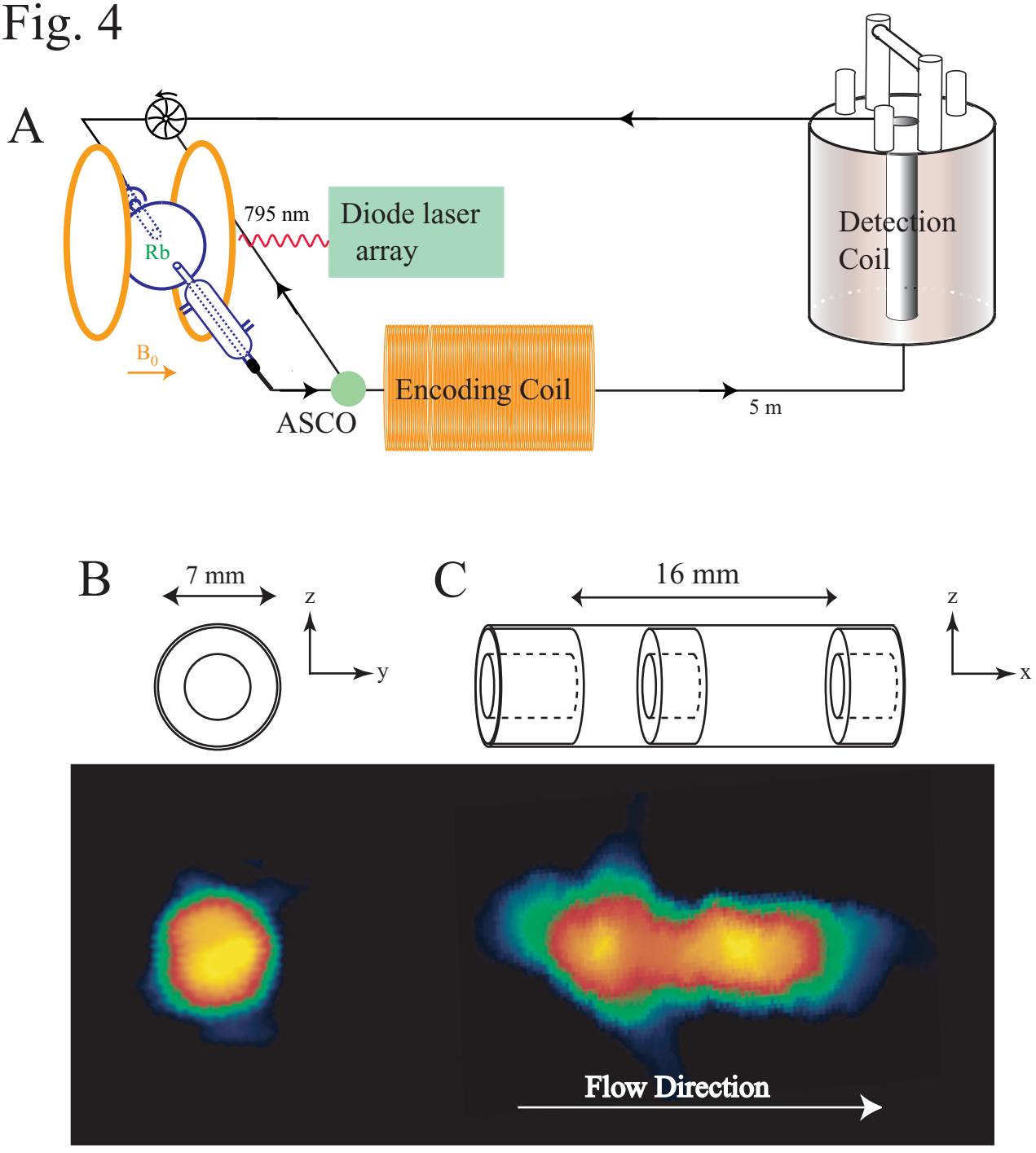
A
795 nm
Diode laser array
Rb
B_0
ASCO
Encoding Coil
5 m
Detection Coil
B
7 mm
z
y
C
16 mm
z
x
Flow Direction